

# A highly shape-adaptive, stretchable design based on conductive liquid for energy harvesting and self-powered biomechanical monitoring

Fang Yi,<sup>1,2\*</sup> Xiaofeng Wang,<sup>2,3\*</sup> Simiao Niu,<sup>2\*</sup> Shengming Li,<sup>2</sup> Yajiang Yin,<sup>3</sup> Keren Dai,<sup>3</sup> Guangjie Zhang,<sup>1</sup> Long Lin,<sup>2</sup> Zhen Wen,<sup>2</sup> Hengyu Guo,<sup>2</sup> Jie Wang,<sup>2</sup> Min-Hsin Yeh,<sup>2</sup> Yunlong Zi,<sup>2</sup> Qingliang Liao,<sup>1</sup> Zheng You,<sup>3</sup> Yue Zhang,<sup>1†</sup> Zhong Lin Wang<sup>2,4†</sup>

The rapid growth of deformable and stretchable electronics calls for a deformable and stretchable power source. We report a scalable approach for energy harvesters and self-powered sensors that can be highly deformable and stretchable. With conductive liquid contained in a polymer cover, a shape-adaptive triboelectric nanogenerator (saTENG) unit can effectively harvest energy in various working modes. The saTENG can maintain its performance under a strain of as large as 300%. The saTENG is so flexible that it can be conformed to any three-dimensional and curvilinear surface. We demonstrate applications of the saTENG as a wearable power source and self-powered sensor to monitor biomechanical motion. A bracelet-like saTENG worn on the wrist can light up more than 80 light-emitting diodes. Owing to the highly scalable manufacturing process, the saTENG can be easily applied for large-area energy harvesting. In addition, the saTENG can be extended to extract energy from mechanical motion using flowing water as the electrode. This approach provides a new prospect for deformable and stretchable power sources, as well as self-powered sensors, and has potential applications in various areas such as robotics, biomechanics, physiology, kinesiology, and entertainment.

## INTRODUCTION

The fast development of deformable and stretchable electronics that exceed the scope of traditional technologies has raised a significant challenge for inventing power sources for such devices (1–4). A shape-adaptive and stretchable energy harvester is a solution because of its ability to accommodate arbitrary surfaces. There are various types of energy harvesters, for example, solar cells that work under sunlight, thermoelectric generators that require a heat source with a temperature gradient, electromagnetic generators that need strong magnetic fields, and piezoelectric generators that are intrigued by pressing force (5–9). Triboelectric nanogenerators (TENGs), which harvest ambient mechanical energy based on the coupling of triboelectrification and electrostatic induction, are a promising type of energy harvester because of their simple fabrication, low cost, light weight, high energy conversion efficiency, and environmentally friendly processes (10–15). Moreover, this type of energy harvester can serve as a self-powered sensor to detect chemicals, pressure, acoustic waves, and motion, which use ambient energy to drive the operation themselves (16–20). Recently, efforts have been made to advance the development of the shape-adaptive and stretchable energy harvesters (21–24). However, these devices have confined stretchability, limited deformable ability, and restricted scalability, which cannot satisfy the requirements imposed by the rapid growth of deformable and stretchable electronics.

Here, we introduce an approach that substantially expands the stretchability, refines the deformable ability, and extends the scalability

of energy harvesters and self-powered sensors. This approach was realized through a shape-adaptive TENG (saTENG) unit composed of a conductive liquid electrode and an elastic polymer cover. Taking advantage of the unique conformability of the liquid electrode, as well as the high flexibility of the rubber cover, the saTENG is capable of withstanding a strain of as large as 300% without degradation of the electrical properties. In addition, water can act as the liquid electrode for the saTENG, which considerably broadens the range of its applications. The saTENG was applied as a wearable energy scavenger and a self-powered biomechanical motion sensor by incorporating with the human body. Furthermore, the saTENG was used for large-area energy harvesting and energy conversion out of mechanical motion using flowing water as the electrode. This work opens up new design opportunities for energy harvesters, stretchable electronics, wearable devices, and self-powered sensors.

## RESULTS

The basic saTENG unit consists of a conductive liquid electrode inside and a rubber layer outside, as schematically shown in Fig. 1A. The rubber layer has a thickness of 200  $\mu\text{m}$ , and its surface was dry-etched to create nanorod structures via inductively coupled plasma (ICP) (25). The surface of the rubber has intrinsic wrinkled structures, and the etched nanorods on the rubber surface have a diameter of  $\sim 50$  nm (Fig. 1B). The nanostructures on the rubber surface can enhance the triboelectric charge density on the surface and increase the effective surface area (26, 27). The conductive liquid inside the rubber can be a conductive solution, liquid metal, or water. Sodium chloride (NaCl) solution and water were chosen to act as electrode materials in this work because they are renewable, low-cost, and environment-friendly. Figure 1C shows an optical picture of a typical saTENG unit; the detailed fabrication process is presented in Materials and Methods.

<sup>1</sup>State Key Laboratory for Advanced Metals and Materials, School of Materials Science and Engineering, and Beijing Municipal Key Laboratory of New Energy Materials and Technologies, University of Science and Technology Beijing, Beijing 100083, China. <sup>2</sup>School of Materials Science and Engineering, Georgia Institute of Technology, Atlanta, GA 30332–0245, USA. <sup>3</sup>Department of Precision Instrument, Tsinghua University, Beijing 100084, China. <sup>4</sup>Beijing Institute of Nanoenergy and Nanosystems, Chinese Academy of Sciences, Beijing 100083, China.

\*These authors contributed equally to this work.

†Corresponding author. Email: yuezhang@ustb.edu.cn (Y.Z.); zlwang@gatech.edu (Z.L.W.)

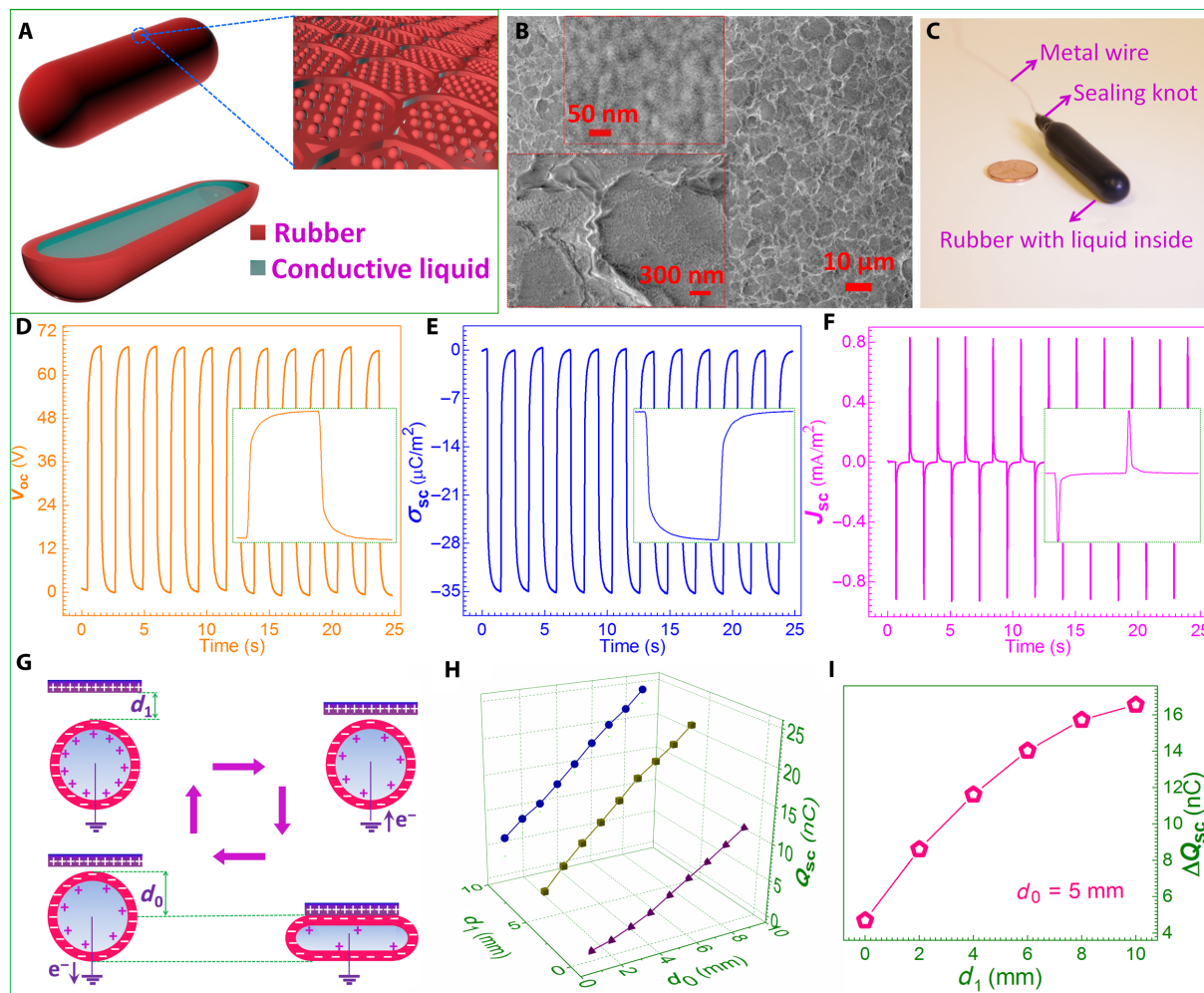


**Fig. 1. Structure of the saTENG unit and its operation in single-electrode mode.** (A) Schematic diagram showing the saTENG unit that is composed of two parts. The zoom-in illustration (top right) shows the nanostructured rubber surface. (B) Scanning electron microscopy images of the rubber surface with dry-etched nanorod structures. (C) Photograph of a typical saTENG unit with a copper wire connecting the conductive liquid. (D to F) The measured typical electrical responses of the saTENG unit working in the single-electrode mode: (D) open-circuit voltage ( $V_{oc}$ ), (E) short-circuit charge density ( $\sigma_{sc}$ ), and (F) short-circuit current density ( $J_{sc}$ ). (G) Schematic illustration of the operating mechanism for the single-electrode-mode saTENG. (H) Dependence of the amount of the transferred short-circuit charge ( $\Delta Q_{sc}$ ) on the deformation of the saTENG unit. (I) Dependence of the  $\Delta Q_{sc}$  on the interval between the nylon and rubber when the deformation degree of the saTENG is the same at each operating cycle.

When the conductive liquid electrode inside the saTENG unit is connected to the ground through a load, it will work in the single-electrode mode to extract energy from mechanical motion. The typical electrical signals of the single-electrode-mode saTENG [diameter, 12.7 mm; length, 50 mm; NaCl solution (20 wt %) as the electrode] are presented in Fig. 1 (D to F). When the saTENG was periodically touched by a nylon film at a frequency of  $\sim 0.45$  Hz, it exhibited an open-circuit voltage ( $V_{oc}$ ) of  $\sim 67.71$  V, a transferred charge density ( $\Delta\sigma_{sc}$ ) of  $\sim 35.35 \mu\text{C}/\text{m}^2$ , and a short-circuit current density ( $J_{sc}$ ) of  $\sim 0.83 \text{ mA}/\text{m}^2$ . The resistance of the liquid electrode is defined as

$$R = \frac{L}{\sigma A} \quad (1)$$

where  $L$  is the length of the liquid electrode,  $A$  is the cross-sectional area of the liquid electrode, and  $\sigma$  is the electrical conductivity of the liquid electrode. During the contact/release motion, the length of the liquid electrode remains the same; therefore, the resistance of the saTENG unit is unchanged. It has been found that when the liquid electrode is nonconductive (paraffin oil, resistance  $>20,200$  gigohms), there will be no electrical outputs under the same experimental condition (fig. S1). It should be noted that the paraffin oil can infiltrate into the rubber in a very slow process, and the NaCl solution has no reaction with the rubber. Hence, both devices were tested immediately after fabrication to ensure equal dimensions of the two devices.

The mechanism of the single-electrode-mode saTENG is shown in Fig. 1G. Note that the acrylic plate that the device was placed onto was

omitted for simplification. When the rubber comes into contact with a material having a lower electron affinity, electrons will be injected to the rubber owing to the triboelectric effect, resulting in surface triboelectric charges. Note that the generated negative triboelectric charges will be retained on the rubber surface for a long period (28). Because of the electrostatic effect, when the positively charged material approaches the rubber, the electric potential of the liquid electrode will rise under the open-circuit condition, and electrons will flow from the ground to the conductive liquid under the short-circuit condition. The electric potential of the liquid electrode and the transferred charges from the ground to the liquid electrode will both reach their maximum values when the approaching material stops moving forward. Then, as the material moves away from the rubber, the electric potential of the liquid electrode will drop under the open-circuit condition, which results in a negative electric potential of the liquid electrode and causes electrons to flow back to the ground under the short-circuit condition. When the material gets back to its initial position, the triboelectric charge distribution of the saTENG will return to its original state. This is an entire working cycle, and an alternating current will be produced as the electrons flow back and forth between the liquid electrode and the ground.

When the distance ( $d_1$ ) between the approaching material (nylon) and the rubber remains the same, the amount of short-circuit transferred charge ( $\Delta Q_{sc}$ ) increases with the increasing deformation ( $d_0$ ) of the saTENG unit (Fig. 1H), and so does  $V_{oc}$  (fig. S2A). This is because as the deformation of the saTENG increases, the contact area between the nylon and the saTENG unit increases, resulting in higher outputs (29, 30). When the deformation of the saTENG unit remains the same at each operation cycle, increasing the distance between the nylon and the rubber also leads to an increase in  $\Delta Q_{sc}$  and  $V_{oc}$  (Fig. 1I and fig. S2B). When  $d_1$  and  $d_0$  remain the same,  $V_{oc}$  and  $\Delta Q_{sc}$  are nearly unchanged, whereas the short-circuit current ( $I_{sc}$ ) ( $I_{sc} = dQ_{sc}/dt$ ) increases with the increasing contact frequency of the rubber and nylon (fig. S3). With the increasing length or diameter of the saTENG unit, both  $V_{oc}$  and  $\Delta Q_{sc}$  increase (figs. S4 and S5), which we attribute to the increasing contact area between the two triboelectric surfaces. If the thickness of the rubber cover increases,  $V_{oc}$  and  $\Delta Q_{sc}$  will both decrease when  $d_1$  and  $d_0$  remain the same (fig. S6). This is because the distance between the nylon surface and the liquid electrode increases when the rubber thickness increases, and thus, the capacitance between the nylon surface and the liquid electrode decreases, resulting in a lower electrical output (31).

In addition to the single-electrode mode, the saTENG unit can also be applied to work in other modes, such as the attached-electrode mode (contact and sliding) and the freestanding mode. In these modes, the periodical relative displacement between the two triboelectric parts (vertical direction for the attached-electrode contact mode and horizontal direction for the attached-electrode sliding mode and the freestanding mode) induces variation of the electric potential difference between the two electrodes under the open-circuit condition, which drives electrons to flow back and forth between the two electrodes through the external load (Fig. 2, F and H, and fig. S7). The simulation results agree with the working principle described in Fig. 2E and fig. S8. Detailed information for all the simulation modeling can be found in note S1. The working principle is further confirmed by the fact that when the connection polarity to the electrometer is switched, the measured  $V_{oc}$  and  $Q_{sc}$  signals will be completely reversed. Like the single-electrode-mode saTENG, the outputs

for saTENGs working in other modes increase when the relative displacement between the two triboelectric parts increases (Fig. 2, C, G, and I). Among those modes, the saTENG working in the single-electrode mode reveals lower-output performance (Fig. 2C) because the electrostatic shield effect of the primary electrode has a negative effect on the performance of the single-electrode-mode TENG (31). The output power of a TENG to the load depends on the impedance match between the load and the power source. At a load resistance of  $\sim 300$  megohms, the attached-electrode contact-mode saTENG reaches a maximum instantaneous power density of  $\sim 200$  mW/m<sup>2</sup> at a frequency of  $\sim 3$  Hz (Fig. 2D). It should be noted that the  $\sim 300$ -megohm-matched inherent impedance of the saTENG is affected by the frequency of the external motion and the inherent capacitance of the saTENG (note S2). Each working mode for the saTENG unit has its own advantages. The single-electrode-mode saTENG has the easiest structure and can conveniently harvest various sources of energy because the other triboelectric part can move freely. The attached-electrode-mode saTENG can provide higher outputs because it is harder to reach air breakdown conditions. The freestanding-mode saTENG can efficiently and conveniently scavenge energy from sliding motion with no constraint to one triboelectric part. In the following paragraphs, we used the single-electrode-mode saTENG to investigate the performance characteristics and demonstrate the applications for the saTENG.

When the NaCl solution was used as the liquid electrode,  $V_{oc}$  and  $\Delta Q_{sc}$  of the saTENG were slightly enhanced with the increasing weight concentration of the NaCl solution (Fig. 3, A and D). This enhancement resulted from the increasing conductivity of the NaCl solution (Fig. 3, B and E, and fig. S9). The resistances of the liquid electrodes at different concentrations can be obtained through Eq. 1, and the decreasing outputs with the increasing resistance are shown in Fig. 3 (C and F). Therefore, for future performance improvement of TENG based on liquid electrodes, it is better to use a liquid with a high conductivity and to minimize the length/cross-sectional area ratio of the liquid electrode. It is noteworthy that when the weight concentration of the NaCl solution is zero (distilled water), the saTENG still exhibits good performance. This is because the inherent impedance for the TENG is typically hundreds of megohms (note S2), whereas the resistance of the distilled water electrode (diameter, 12.7 mm; length, 50 mm) is  $\sim 10.8$  kilohms, which is much smaller than the inherent impedance. For TENG, this high inherent impedance allows the resistance of its electrode to vary within a wide range without much degradation of the performance (note S3). Furthermore, the high inherent impedance of the saTENG also leads to a low potential difference across the liquid electrode, which saves the liquid from being electrolyzed (note S3).

The saTENG can maintain its high performance after being stretched by 300%. As shown in Fig. 3 (G to I), with the elongation of the saTENG,  $V_{oc}$  and  $\Delta Q_{sc}$  initially increase and then slightly decrease. The output signals were acquired from the contact/release interaction between the rubber and an acrylic plate, with the same deformation of the saTENG at different stretched lengths. The experimental setup for the stretchability test can be found in Materials and Methods and fig. S10. The contact area between the rubber and the acrylic can be calculated as

$$S = w_x L_0 (1 + \varepsilon) \quad (2)$$

where  $w_x$  is the width of the contact area between the acrylic and the rubber of the saTENG unit,  $L_0$  is the length of the saTENG unit in the

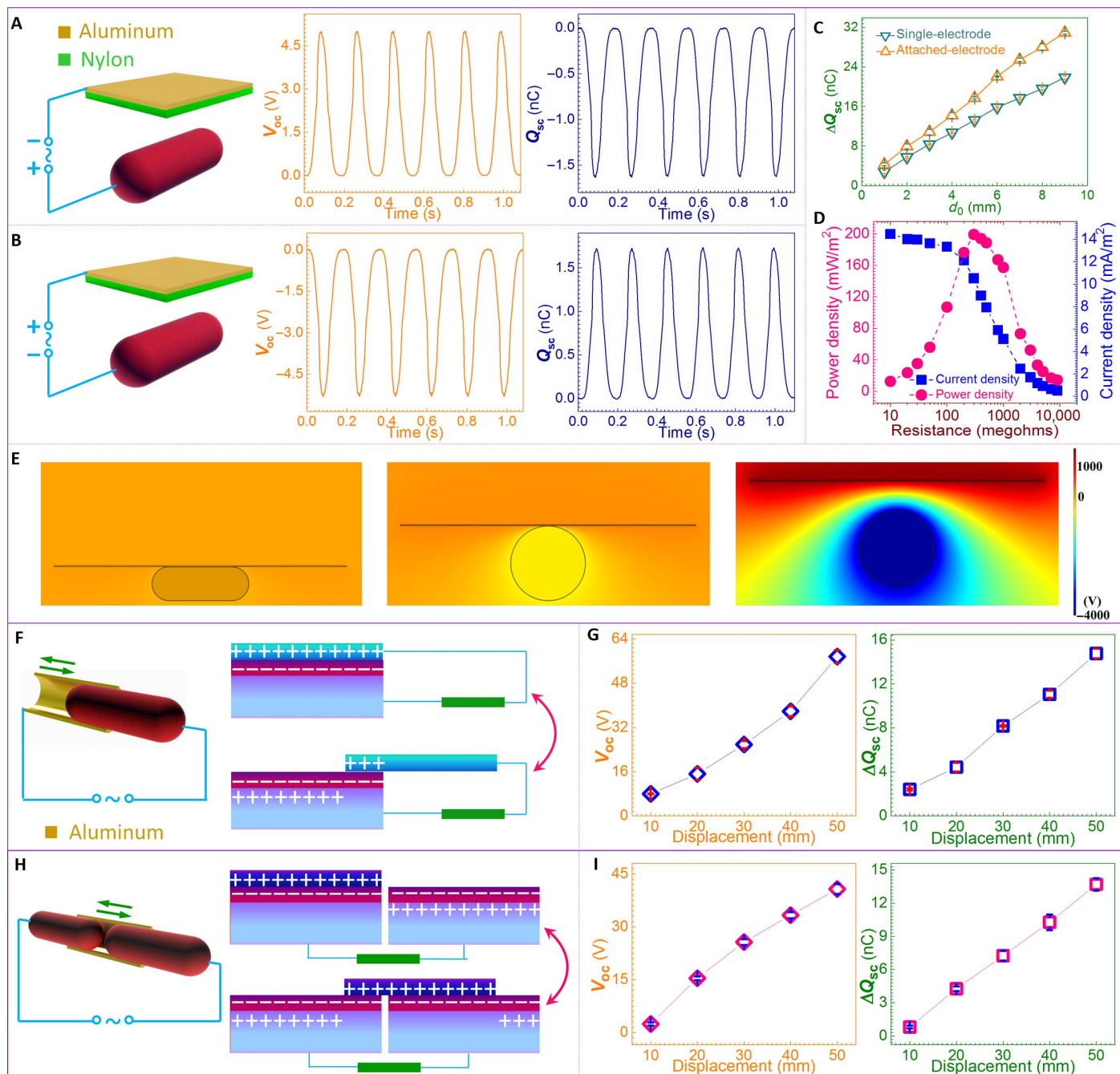


**Fig. 2. Investigation of the saTENG unit working in other modes.** (A and B) The open-circuit voltage ( $V_{oc}$ ) and short-circuit transferred charge ( $Q_{sc}$ ) of the attached-electrode contact-mode saTENG with (A) forward connection and (B) reverse connection to the liquid electrode. (C) Comparison of the  $\Delta Q_{sc}$  of the saTENG working in the single-electrode mode and attached-electrode mode (contact/release motion,  $d_1 = 5$  mm). (D) Load matching test of the saTENG working in the attached-electrode contact mode at a frequency of  $\sim 3$  Hz. Maximum average output power is obtained at a matched load of  $\sim 300$  megohms. (E) Simulation results for the attached-electrode contact-mode saTENG exhibit the increasing electrical potential difference between the liquid electrode and the aluminum electrode as the distance between the rubber and nylon increases. Note that for simplification, the acrylic plate support under the saTENG unit is omitted in the simulation model, which will not affect the changing trend of the electrical potential due to the superposition principle of electrical potential. (F and G) Working mechanism (F) and dependence (G) of  $V_{oc}$  and  $\Delta Q_{sc}$  on the sliding displacement for the saTENG unit operating in the attached-electrode sliding mode. (H and I) Working mechanism (H) and dependence (I) of  $V_{oc}$  and  $\Delta Q_{sc}$  on the parallel-moving displacement for the saTENG unit operating in the freestanding mode.

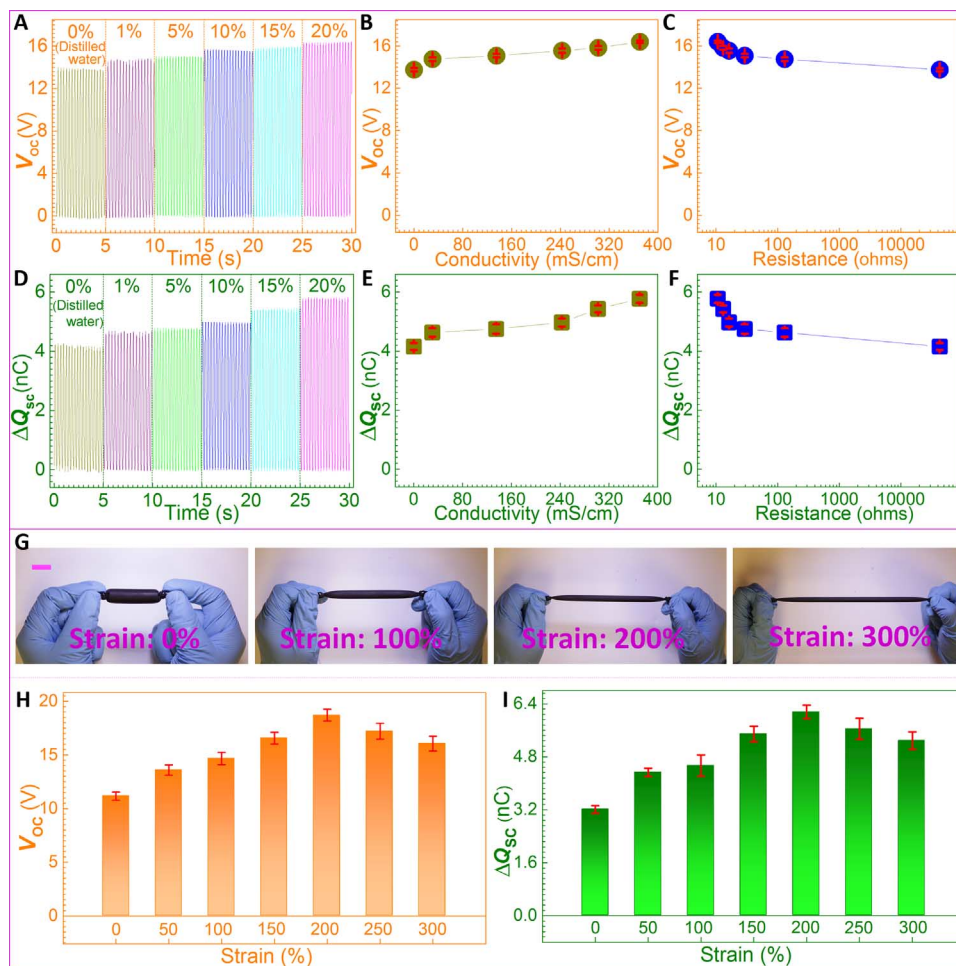


**Fig. 3. Influences of liquid conductivity, liquid electrode resistance, and saTENG elongation on performance.** (A and D) The measured open-circuit voltage ( $V_{oc}$ ) (A) and the amount of short-circuit transferred charge ( $\Delta Q_{sc}$ ) (D) of saTENGs with electrodes of different NaCl weight concentrations. (B and E) Dependence of  $V_{oc}$  (B) and  $\Delta Q_{sc}$  (E) on the conductivity of the liquid electrode. (C and F) Dependence of  $V_{oc}$  (C) and  $\Delta Q_{sc}$  (F) on the resistance of the liquid electrode. (G) Photographs showing the saTENG under different tensile strains. Scale bar, 2 cm. (H and I) Dependence of  $V_{oc}$  (H) and  $\Delta Q_{sc}$  (I) on the tensile strain of the saTENG.

original state, and  $\epsilon$  is the tensile strain of the saTENG unit. The contact area between the acrylic and the rubber increases with the stretched saTENG (note S4), which contributes to the enhancement of the outputs. The resistance of the liquid electrode of the elongated saTENG can be calculated as

$$R_S = \frac{L_0(1 + \epsilon)^2}{\sigma A_0} \quad (3)$$

where  $A_0$  is the cross-sectional area of the saTENG at the original state. The deduction of Eq. 3 can be found in note S5. It is clear that the resistance of the liquid electrode increases with the elongation. It should be noted that the stretched device in the experiment has two cone-shaped ends because the two ends are bound. Therefore, the real contact area between the acrylic and the rubber will be smaller than the calculated contact area from Eq. 2, and the real resistance of

the liquid electrode of the stretched device will be larger than the calculated resistance from Eq. 3. As mentioned above, a larger resistance of the liquid electrode results in a slightly lower output, whereas a bigger contact area leads to a higher output. At small tensile strain, the increasing contact area plays a dominant role in the performance; therefore, the electrical outputs of the saTENG keep increasing. As the tensile strain increases; because of the two cone-shaped ends of the stretched saTENG unit, the increasing rate of the contact area reduces, whereas the increasing rate of the resistance increases. As a result, the negative effect on the performance by the increasing resistance will outstrip the positive effect on the performance by the increasing contact area. Hence, the electrical outputs of the saTENG stop increasing and start to decline. In an extreme case where the saTENG is stretched to an infinite length, the resistance of the liquid electrode will approach infinity, and the saTENG will present nearly no electrical outputs. Therefore, it could be predicted that the electrical outputs will follow a very slowly decreasing trend if the saTENG

unit is further stretched. The same changing trend of  $V_{oc}$  and  $\Delta Q_{sc}$  agrees with the common relationship between  $V_{oc}$  and  $\Delta Q_{sc}$  of a TENG (31)

$$V_{oc} = \frac{\Delta Q_{sc}}{C} \quad (4)$$

where  $C$  is a constant for the single-electrode-mode saTENG. The excellent stretchability of the saTENG is attributed to the unique ability of the liquid to conform to the shape of its container and the high flexibility of the rubber cover. For practical use, saTENGs with specified shapes and stretchability can be developed or custom-tailored by using suitable covers.

Because there is no chemical reaction between the NaCl solution (or the water) and the rubber, the durability and reliability of the saTENG unit depend on the rubber cover. There is no obvious degradation of the output electrical signals of the saTENG under the original state or the stretched state (tensile strain, 300%) after ~55,000 deformation cycles (figs. S11 and S12), which indicates good reliability and stability of the saTENG in operation.

The stretchable saTENG has a wide range of applications in everyday life. It can not only tolerate arbitrary surfaces but also accommodate movable parts. Figure 4 (A to C) shows the application of the saTENG to harvest energy from human walking and to monitor foot

motion. As shown in Fig. 4A, a saTENG was mounted under the shoe like a shoe pad, with tap water (conductivity, 0.248 mS/cm) as the liquid electrode. Note that the human body, which is a sizeable, good conductor, served as the ground for all the wearable saTENGs shown in Fig. 4, and tap water was used as the electrode for all the saTENGs in the demonstrated applications. Two groups of light-emitting diodes (LEDs) with reversed polarity were used to visualize foot motion (Fig. 4B). Note that the equivalent circuit diagrams for the LED arrays in other demonstrations can be found in fig. S13. The two groups of LEDs were lighted up alternately while the foot was up and down during human walking. When the foot is up, the declined electric potential of the water electrode causes electrons to flow from the water electrode to the ground, lighting the upper group of LEDs; when the foot is pressed down, the raised electric potential of the water electrode drives electrons to transfer from the ground to the water electrode, lighting the lower group of LEDs (Fig. 4C and movie S1). This kind of outsole saTENG can be applied in areas such as robotics and entertainment. As shown in Fig. 4D and movie S2, a bracelet-like saTENG was worn on a human wrist to harvest energy from tapping motion. Under a tapping cycle, the saTENG can drive more than 80 LEDs, indicating its effectiveness as a wearable power source. The electricity generated from the saTENG can also be stored in energy storage devices such as capacitors and batteries after a rectification of the alternate current signals. Figure 4E and movie S3 present the process of the saTENG storing the harvested energy into

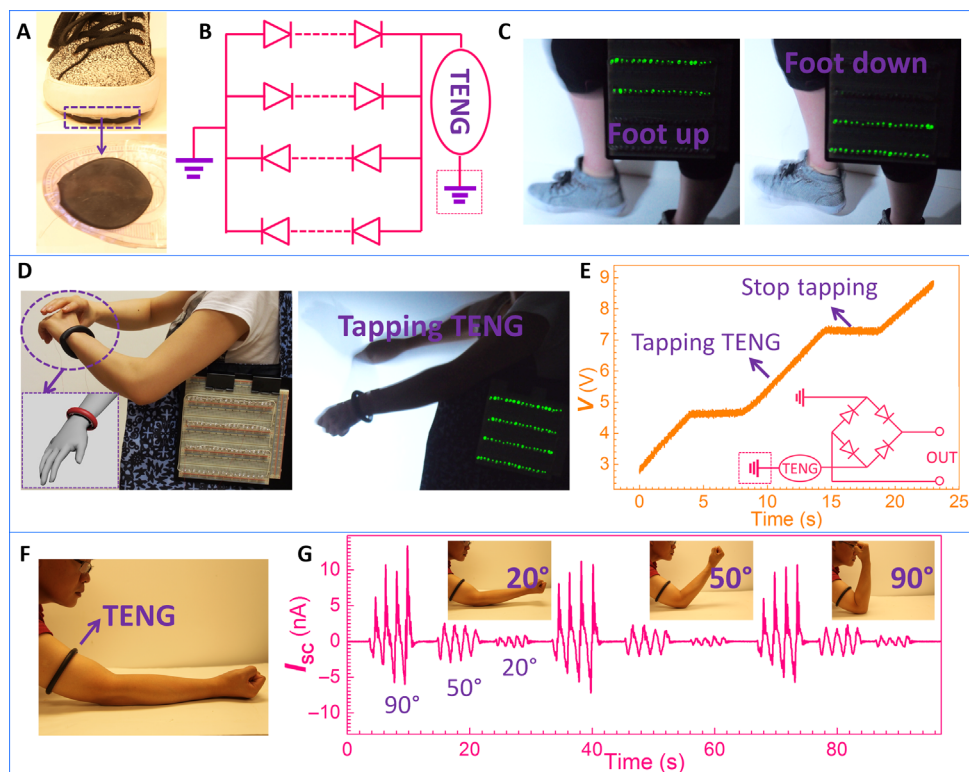


**Fig. 4. Demonstrations of the saTENG as a wearable energy harvester and self-powered biomechanical monitor.** (A to C) A saTENG attached to a shoe to extract energy from foot motion: (A) photograph of the pedal-like saTENG sited under the shoe; (B) equivalent electric circuit diagram depicting the order of the LED serials; and (C) photograph showing the LEDs driven by foot motion. (D to G) A saTENG looped around the arm of a subject to harvest energy from tapping motion and serve as self-powered arm motion sensor: (D) photographs showing LEDs driven by tapping the bracelet-like saTENG; (E) charging a capacitor with the brace-like saTENG; (F) the saTENG worn on the upper arm; (G) response of the saTENG to different bending angles.

a capacitor (aluminum electrolytic capacitor, 1  $\mu\text{F}$ ). An integrated low-loss full-wave bridge rectifier was connected between the saTENG and the capacitor to achieve the energy storage process. The voltage of the capacitor quickly increases ( $\sim 25$  V/min) when the saTENG is tapped and becomes flat once the tapping motion stops. Besides functioning as a wearable power source, the bracelet-like saTENG can serve as a self-powered body motion sensor. As shown in Fig. 4 (F and G) and movie S4, a bracelet-like saTENG was worn around the upper arm, and it is capable of detecting the bending angle of the forearm when doing bicep curls. The volume of the biceps increases when the elbow is bent and recovers when the arm is extended, leading to a change in the upper arm circumference and therefore an alteration of the contact area between the saTENG and the arm skin. The periodic change in the contact area induces a stream of electrons to flow back and forth between the water electrode of the saTENG and the ground. The contact area increases when the bending angle is enlarged, bringing about a larger amount of the transferred electrons and thus a higher output current under the same bending rate. This bracelet-like saTENG feels soft and comfortable, and it can be worn as an accessory. Because of its portability, convenience, low cost, easy fabrication, and aesthetic value, it has promising applications such as emergency response and exercise monitoring.

Moreover, the saTENG can be extended to act as a large-area energy harvester because of its highly scalable fabrication process and the abundance of water on Earth. As shown in Fig. 5A, a water cushion with a size of  $183 \times 69 \times 5$  cm was used to harvest mechanical energy. The cushion cover had a thickness of  $\sim 900$   $\mu\text{m}$ , and the inner water was connected to the LEDs with a metal wire. A large piece of metal served as the ground for the large-area saTENG. When the water cushion is patted with an acrylic plate ( $8 \times 13$  cm), the saTENG is capable of driving 170 LEDs (Fig. 5B and movie S5). Note that the acrylic plate can be replaced by other materials such as human skin (movie S6). This cushion-like energy harvester could be useful in entertainment, sports, and architectural designs. In addition, the saTENG could be further extended to harvest mechanical energy, using flowing water as the electrode. When the water driven by a syringe pump ran through a rubber tube (diameter, 6.3 mm; length, 55 mm), tapping the rubber tube generated electrical output signals. The working mechanism of the saTENG with a flowing water electrode is the same as that with a bound water electrode;  $V_{oc}$  and  $\Delta Q_{sc}$  increase when the deformation of the rubber tube increases (the interval between the acrylic plate and the rubber tube is the same) (Fig. 5, C and D). Figure 5 (E and F) demonstrates the application of the saTENG to extract mechanical energy based on household plumbing. As shown in Fig. 5E, one end of the serial LED was connected to the running water in the

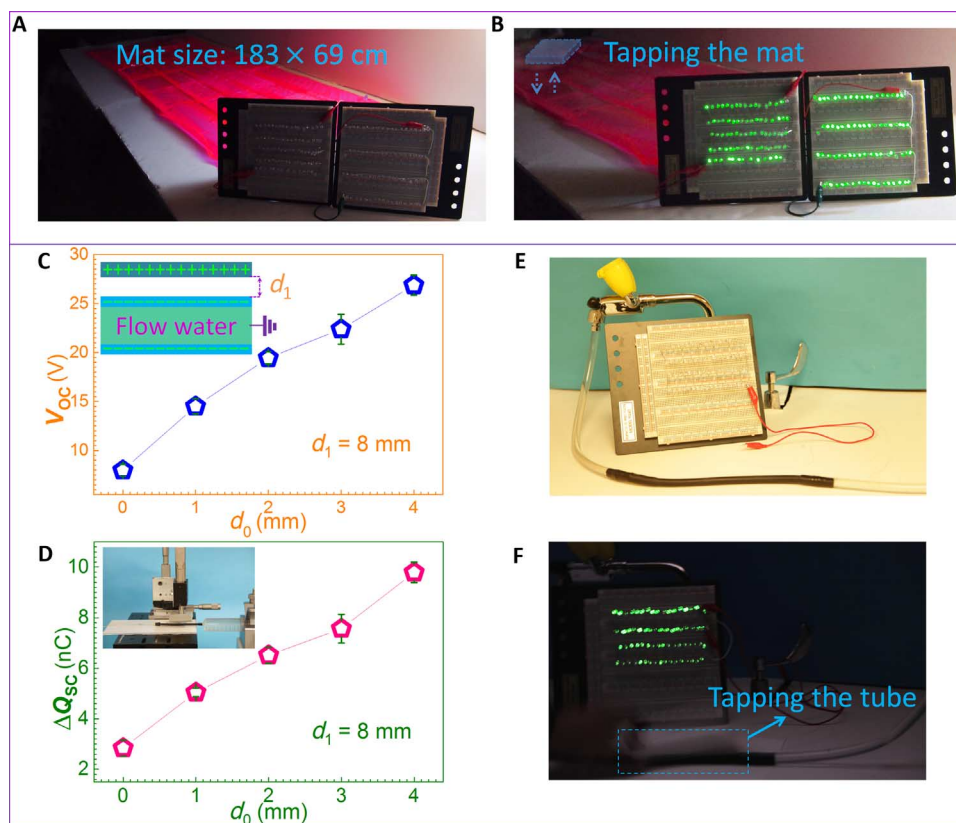


**Fig. 5. Demonstrations of the saTENG for large-area energy conversion and to harvest energy, using flowing water as the electrode.** (A) Photograph showing the experimental arrangement for a water cushion extracting energy from mechanical motion. (B) Photograph showing that  $\sim 170$  LEDs were lighted up by tapping the water cushion. (C and D) The increasing outputs with the increasing deformation of the water tube: (C) the open-circuit voltage ( $V_{oc}$ ) and (D) the amount of short-circuit transferred charge ( $\Delta Q_{sc}$ ). (E) Photograph showing the experimental arrangement for the saTENG harvesting mechanical energy based on household plumbing. (F) Photograph showing that  $\sim 80$  LEDs were lighted up by tapping the rubber pipe with flowing water as the electrode.

pipe, and the other end was connected to the ground (human body or a large piece of metal, excluding the metal plumbing that delivered the water). When the rubber tube was patted with an acrylic plate, dozens of LEDs were lit up (Fig. 5F and movie S7).

The sliding and freestanding modes for the saTENG unit can also be applied to harvest energy from the motions used in everyday life, such as arm swing, hand movement, and human walking. By mounting a saTENG on the upper human body (fig. S14, A and B), the normal swing motion of the arm causes electrons to flow back and forth between the water electrode and the ground (human body) for the saTENG working in the single-electrode sliding mode (fig. S14A) or between the water electrode and the other electrode for the saTENG working in the attached-electrode sliding mode (fig. S14B), both of which can effectively light up dozens of LEDs (movies S8 and S9). For the applications of the freestanding mode, we demonstrate that by moving a mouse on two adjacent water mouse pads (fig. S14C) or walking across two water mats (fig. S14D), electrons will flow back and forth between the two water electrodes of the water mouse pads or water mats, which can also effectively light up LEDs (movies S10 and S11).

## DISCUSSION

The concept presented here enables energy harvesters and self-powered sensors with high deformability and stretchability. The unique capability of liquid to conform to the shape of its container endows the energy harvester with theoretically limitless deformation and stretchability. The energy harvester has a highly scalable manufacturing process, which makes it feasible for small- and large-scale applications. The energy harvester can also serve as a self-powered sensor to monitor biomechanical motion. For practical use, cover material for the liquid electrode with specified properties could be selected to suit the actual needs; for a high-output performance, it is advisable to choose materials tending to be readily charged by friction for the container and minimize the resistance of the liquid electrode.

In addition, the high inherent impedance of the fabricated energy harvester allows the resistance of its electrode to vary within a wide range. This high impedance also results in a low potential difference across the liquid electrode, which saves the liquid from being electrolyzed. It has been demonstrated that water can be used as the electrode for the energy harvester, which cuts down the cost of production and significantly expands the applications owing to the abundance of water on Earth. The energy harvester could also be extended to scavenge mechanical energy using flowing water as the electrode. This way of harvesting water-related energy is different from traditional techniques for harvesting water energy, which usually rely on the direct interaction of the water with another material or the potential gradient induced by the dissolved ions in water (32–36). Thus, this platform may provide a new route for harvesting water-related energy.

This approach is also human-friendly and skin-compatible. It is predicted that this concept will be useful in wearable electronics, haptic sensation, implantable devices, emergency response, architectural designs, sports, robotics, and entertainment. Future work along this direction could involve further improvement of the output performance through maximizing surface charge density of the cover material and optimizing the device structure, integration with energy storage devices for sustainable power supply systems, development of self-

powered stretchable sensors, and construction of self-powered stretchable electronics systems.

## MATERIALS AND METHODS

### Materials

Paraffin oil and sodium chloride ( $\geq 99.5\%$ ) were purchased from Sigma-Aldrich. The rubber is a commercial product produced by Qualatex. The nanostructures on the rubber surface were created via the ICP method; the etching time was 50 s. The flow rates of Ar, O<sub>2</sub>, and CF<sub>4</sub> gases were 15.0, 10.0, and 30.0 sccm, respectively. An aluminum film on top of a nylon film was deposited by sputtering. The water cushion was fabricated through injecting water into an inflatable swimming pool mat. The 5-mm green LEDs in Figs. 4 and 5 were made by Nichia (LED type: NSPG500DS). The 10-mm green LEDs in fig. S14 were made by Riysm ( $V_F$ , 3.0 to 3.2 V;  $I_F$ , 15 to 20 mA).

### Fabrication of the shape-adaptive, stretchable energy harvester unit

(i) A hollow cylindrical rubber layer (thickness, 200  $\mu\text{m}$ ) with one end open and the other closed was initially washed thoroughly with ethanol and distilled water and then blown dry with nitrogen. (ii) Conductive liquid (sodium chloride solution or water) was injected into the rubber container. (iii) A copper wire was dipped into the conductive liquid. (iv) A knot was tied at the open end of the cylindrical rubber container to seal up the liquid.

### Experimental setup for the shape-adaptive, stretchable energy harvester

**The contact/release motion for saTENGs working in the single-electrode contact mode and attached-electrode contact mode.** The nylon film (50 mm  $\times$  50 mm  $\times$  100  $\mu\text{m}$ ) was attached to an acrylic plate, which was mounted onto a linear motor. Note that for the attached-electrode contact mode, a 150-nm aluminum film was deposited on top of the nylon film, which served as the other electrode. The saTENG unit was placed onto another acrylic plate perpendicular to the moving direction of the motor, with its two ends bound by foam tape. The reciprocating motion of the linear motor stimulated the contact/release motion. To test the influence of the contact frequency, a shaker (Labworks SC-121) was applied to drive the contact/release motion.

**The sliding motion for saTENGs working in the attached-electrode sliding mode and freestanding mode.** One (attached-electrode sliding mode) or two (freestanding mode) saTENG units were placed under the linear motor. An aluminum layer (thickness, 50  $\mu\text{m}$ ) was attached to a semiround acrylic pipe that was fixed on the linear motor. The movement of the linear motor led to the moving of the aluminum over the saTENG unit(s).

**Stretchability test.** The saTENG unit was placed onto an acrylic plate, and another acrylic plate with the same length as the stretched saTENG was attached onto a linear motor. Two ends of the saTENG were bound with narrow tape, which controlled the elongation of the saTENG. The linear motor was used to induce the contact/release motion (fig. S10).

### Measurement

The morphology of the nanostructured rubber surface was characterized by a field emission scanning electron microscope (Hitachi SU8010).

The conductivity of the liquid was obtained from the measured resistance of a cubic centimeter of liquid, which was acquired through the alternating current impedance method by using an electrochemical analyzer/workstation. The voltage, charge, and current of the saTENGs were measured by a programmable electrometer (part no. 6514, Keithley), and the data were collected and recorded by computer-controlled measurement software written in LabVIEW.

## SUPPLEMENTARY MATERIALS

Supplementary material for this article is available at <http://advances.sciencemag.org/cgi/content/full/2/6/e1501624/DC1>

note S1. Detailed information for the simulation modeling.

note S2. Factors affecting TENG's inherent impedance.

note S3. Consequences of the saTENG's high inherent impedance.

note S4. Detailed explanation for the increasing contact area with the increasing elongation of the saTENG.

note S5. Detailed derivation of Eq. 3.

fig. S1. The measured typical electrical responses of the saTENG unit, with paraffin oil as the electrode.

fig. S2. Dependence of the open-circuit voltage ( $V_{oc}$ ) on the deformation of the saTENG unit and the interval between the nylon and rubber.

fig. S3. Influence of the contact frequency of the two triboelectric surfaces on the electrical outputs of the single-electrode-mode saTENG.

fig. S4. Influence of the length of the saTENG unit on the electrical outputs of the single-electrode-mode saTENG.

fig. S5. Influence of the diameter of the saTENG unit on the electrical outputs of the single-electrode-mode saTENG.

fig. S6. Theoretical results of the influence of the thickness of the rubber cover on the electrical outputs of the single-electrode-mode saTENG.

fig. S7. Schematic diagram exhibiting the operating mechanism for the saTENG working in the attached-electrode contact mode.

fig. S8. Simulation results showing the increasing electrical potential difference between the two electrodes for saTENG units working in the attached-electrode sliding mode and freestanding mode.

fig. S9. Increasing conductivity of the NaCl solution with the increasing weight concentration.

fig. S10. Experimental setup for the stretchability test.

fig. S11. Cycle test of the saTENG under the original state.

fig. S12. Cycle test of the saTENG under the stretched state.

fig. S13. Equivalent circuit diagrams for the LED arrays in demonstrations.

fig. S14. Demonstrations of the sliding-mode and freestanding-mode saTENGs to harvest energy from human motion.

movie S1. Harvesting energy from foot motion by an outsole saTENG.

movie S2. A bracelet-like saTENG worn on a human wrist to harvest energy from tapping motion.

movie S3. Charging an aluminum electrolytic capacitor by a bracelet-like saTENG.

movie S4. A bracelet-like saTENG worn on the upper arm to monitor arm motion.

movie S5. Harvesting energy by a large-area cushion-like saTENG tapped by an acrylic plate.

movie S6. Harvesting energy by a large-area cushion-like saTENG touched by human skin.

movie S7. Harvesting mechanical energy based on household plumbing, using flowing water as the electrode.

movie S8. Harvesting energy from arm swing by a saTENG working in the single-electrode sliding mode.

movie S9. Harvesting energy from arm motion by an attached-electrode-mode saTENG.

movie S10. Harvesting energy from moving a mouse by a freestanding-mode saTENG.

movie S11. Harvesting energy from human walking by a freestanding-mode saTENG.

## REFERENCES AND NOTES

- H.-H. Chou, A. Nguyen, A. Chortos, J. W. F. To, C. Lu, J. Mei, T. Kurosawa, W.-G. Bae, J. B.-H. Tok, Z. Bao, A chameleon-inspired stretchable electronic skin with interactive colour changing controlled by tactile sensing. *Nat. Commun.* **6**, 8011 (2015).
- B. C.-K. Tee, C. Wang, R. Allen, Z. Bao, An electrically and mechanically self-healing composite with pressure- and flexion-sensitive properties for electronic skin applications. *Nat. Nanotechnol.* **7**, 825–832 (2012).
- T. Sekitani, H. Nakajima, H. Maeda, T. Fukushima, T. Aida, K. Hata, T. Someya, Stretchable active-matrix organic light-emitting diode display using printable elastic conductors. *Nat. Mater.* **8**, 494–499 (2009).

- M. Kaltenbrunner, T. Sekitani, J. Reeder, T. Yokota, K. Kuribara, T. Tokuhara, M. Drack, R. Schwödiauer, I. Graz, S. Bauer-Gogonea, S. Bauer, T. Someya, An ultra-lightweight design for imperceptible plastic electronics. *Nature* **499**, 458–463 (2013).
- J. M. Donelan, Q. Li, V. Naing, J. A. Hoffer, D. J. Weber, A. D. Kuo, Biomechanical energy harvesting: Generating electricity during walking with minimal user effort. *Science* **319**, 807–810 (2008).
- D. Kraemer, B. Poudel, H.-P. Feng, J. C. Caylor, B. Yu, X. Yan, Y. Ma, X. Wang, D. Wang, A. Muto, K. McEnaney, M. Chiesa, Z. Ren, G. Chen, High-performance flat-panel solar thermoelectric generators with high thermal concentration. *Nat. Mater.* **10**, 532–538 (2011).
- A. Mei, X. Li, L. Liu, Z. Ku, T. Liu, Y. Rong, M. Xu, M. Hu, J. Chen, Y. Yang, M. Grätzel, H. Han, A hole-conductor-free, fully printable mesoscopic perovskite solar cell with high stability. *Science* **345**, 295–298 (2014).
- C. B. Vining, An inconvenient truth about thermoelectrics. *Nat. Mater.* **8**, 83–85 (2009).
- R. Yang, Y. Qin, L. Dai, Z. L. Wang, Power generation with laterally packaged piezoelectric fine wires. *Nat. Nanotechnol.* **4**, 34–39 (2009).
- J. Bae, J. Lee, S. Kim, J. Ha, B.-S. Lee, Y. Park, C. Choong, J.-B. Kim, Z. L. Wang, H.-Y. Kim, J.-J. Park, U.-I. Chung, Flutter-driven triboelectrification for harvesting wind energy. *Nat. Commun.* **5**, 4929 (2014).
- Z. L. Wang, J. Chen, L. Lin, Progress in triboelectric nanogenerators as a new energy technology and self-powered sensors. *Energy Environ. Sci.* **8**, 2250–2282 (2015).
- G. Zhu, J. Chen, T. Zhang, Q. Jing, Z. L. Wang, Radial-arrayed rotary electrification for high performance triboelectric generator. *Nat. Commun.* **5**, 3426 (2014).
- Z. L. Wang, Triboelectric nanogenerators as new energy technology for self-powered systems and as active mechanical and chemical sensors. *ACS Nano* **7**, 9533–9557 (2013).
- G. Zhu, C. Pan, W. Guo, C.-Y. Chen, Y. Zhou, R. Yu, Z. L. Wang, Triboelectric-generator-driven pulse electrodeposition for micropatterning. *Nano Lett.* **12**, 4960–4965 (2012).
- S. Niu, X. Wang, F. Yi, Y. S. Zhou, Z. L. Wang, A universal self-charging system driven by random biomechanical energy for sustainable operation of mobile electronics. *Nat. Commun.* **6**, 8975 (2015).
- J. Yang, J. Chen, Y. Su, Q. Jing, Z. Li, F. Yi, X. Wen, Z. Wang, Z. L. Wang, Eardrum-inspired active sensors for self-powered cardiovascular system characterization and throat-attached anti-interference voice recognition. *Adv. Mater.* **27**, 1316–1326 (2015).
- F. Yi, L. Lin, S. Niu, J. Yang, W. Wu, S. Wang, Q. Liao, Y. Zhang, Z. L. Wang, Self-powered trajectory, velocity, and acceleration tracking of a moving object/body using a triboelectric sensor. *Adv. Funct. Mater.* **24**, 7488–7494 (2014).
- Z.-H. Lin, G. Zhu, Y. S. Zhou, Y. Yang, P. Bai, J. Chen, Z. L. Wang, A self-powered triboelectric nanosensor for mercury ion detection. *Angew. Chem. Int. Ed.* **52**, 5065–5069 (2013).
- L. Lin, Y. Xie, S. Wang, W. Wu, S. Niu, X. Wen, Z. L. Wang, Triboelectric active sensor array for self-powered static and dynamic pressure detection and tactile imaging. *ACS Nano* **7**, 8266–8274 (2013).
- S. Wang, L. Lin, Z. L. Wang, Triboelectric nanogenerators as self-powered active sensors. *Nano Energy* **11**, 436–462 (2015).
- P.-K. Yang, L. Lin, F. Yi, X. Li, K. C. Pradel, Y. Zi, C.-I. Wu, J.-H. He, Y. Zhang, Z. L. Wang, A Flexible, stretchable and shape-adaptive approach for versatile energy conversion and self-powered biomedical monitoring. *Adv. Mater.* **27**, 3817–3824 (2015).
- K. N. Kim, J. Chun, J. W. Kim, K. Y. Lee, J.-U. Park, S.-W. Kim, Z. L. Wang, J. M. Baik, Highly stretchable 2D fabrics for wearable triboelectric nanogenerator under harsh environments. *ACS Nano* **9**, 6394–6400 (2015).
- S. Park, H. Kim, M. Vosgueritchian, S. Cheon, H. Kim, J. H. Koo, T. R. Kim, S. Lee, G. Schwartz, H. Chang, Z. Bao, Stretchable energy-harvesting tactile electronic skin capable of differentiating multiple mechanical stimuli modes. *Adv. Mater.* **26**, 7324–7332 (2014).
- F. Yi, L. Lin, S. Niu, P. K. Yang, Z. Wang, J. Chen, Y. Zhou, Y. Zi, J. Wang, Q. Liao, Y. Zhang, Z. L. Wang, Stretchable-rubber-based triboelectric nanogenerator and its application as self-powered body motion sensors. *Adv. Funct. Mater.* **25**, 3688–3696 (2015).
- H. Fang, W. Wu, J. Song, Z. L. Wang, Controlled growth of aligned polymer nanowires. *J. Phys. Chem. C* **113**, 16571–16574 (2009).
- P. Bai, G. Zhu, Z.-H. Lin, Q. Jing, J. Chen, G. Zhang, J. Ma, Z. L. Wang, Integrated multilayered triboelectric nanogenerator for harvesting biomechanical energy from human motions. *ACS Nano* **7**, 3713–3719 (2013).
- C. K. Jeong, K. M. Baek, S. Niu, T. W. Nam, Y. H. Hur, D. Y. Park, G.-T. Hwang, M. Byun, Z. L. Wang, Y. S. Jung, K. J. Lee, Topographically-designed triboelectric nanogenerator via block copolymer self-assembly. *Nano Lett.* **14**, 7031–7038 (2014).
- F. Saurenbach, D. Wollmann, B. D. Terris, A. F. Diaz, Force microscopy of ion-containing polymer surfaces: Morphology and charge structure. *Langmuir* **8**, 1199–1203 (1992).
- S. Niu, Y. Liu, S. Wang, L. Lin, Y. S. Zhou, Y. Hu, Z. L. Wang, Theoretical investigation and structural optimization of single-electrode triboelectric nanogenerators. *Adv. Funct. Mater.* **24**, 3332–3340 (2014).
- S. Niu, S. Wang, L. Lin, Y. Liu, Y. S. Zhou, Y. Hu, Z. L. Wang, Theoretical study of contact-mode triboelectric nanogenerators as an effective power source. *Energy Environ. Sci.* **6**, 3576–3583 (2013).

31. S. Niu, Z. L. Wang, Theoretical systems of triboelectric nanogenerators. *Nano Energy* **14**, 161–192 (2015).
32. P. Dhiman, F. Yavari, X. Mi, H. Gullapalli, Y. Shi, P. M. Ajayan, N. Koratkar, Harvesting energy from water flow over graphene. *Nano Lett.* **11**, 3123–3127 (2011).
33. Z.-H. Lin, G. Cheng, S. Lee, K. C. Pradel, Z. L. Wang, Harvesting water drop energy by a sequential contact-electrification and electrostatic-induction process. *Adv. Mater.* **26**, 4690–4696 (2014).
34. G. Zhu, Y. Su, P. Bai, J. Chen, Q. Jing, W. Yang, Z. L. Wang, Harvesting water wave energy by asymmetric screening of electrostatic charges on a nanostructured hydrophobic thin-film surface. *ACS Nano* **8**, 6031–6037 (2014).
35. Y. Xie, D. Bos, L. J. de Vreede, H. L. de Boer, M.-J. van der Meulen, M. Versluis, A. J. Sprenkels, A. van den Berg, J. C. T. Eijkel, High-efficiency ballistic electrostatic generator using microdroplets. *Nat. Commun.* **5**, 3575 (2014).
36. F. H. J. van der Heyden, D. J. Bonthuis, D. Stein, C. Meyer, C. Dekker, Power generation by pressure-driven transport of ions in nanofluidic channels. *Nano Lett.* **7**, 1022–1025 (2007).

#### Acknowledgments

**Funding:** The research was supported by the Hightower Chair Foundation and the “Thousands Talents” program (China) for pioneer researcher (Z.L.W.) and his innovation team, the National Natural Science Foundation of China (grant nos. 51432005, 51527802, and 51232001), the National Major Research Program of China (no. 2013CB932602), the Program of Introducing

Talents of Discipline to Universities (B14003), National Natural Science Foundation of China (nos. 51527802 and 51232001), Beijing Municipal Science and Technology Commission, and the Fundamental Research Funds for Central Universities. Patents have been filed on the basis of the research results presented in this article. **Author contributions:** F.Y., Z.L.W., and Y.Z. conceived the idea. F.Y. and X.W. designed the experiments. F.Y., X.W., and S.N. performed the experiments. F.Y., X.W., and S.N. graphed and analyzed the data. F.Y., Z.L.W., S.N., and Y.Z. wrote the paper. All authors discussed the results and commented on the manuscript. **Competing interests:** The authors declare that they have no competing interests. **Data and materials availability:** All data needed to evaluate the conclusions in the paper are present in the paper and/or the Supplementary Materials. Additional data related to this paper may be requested from the authors.

Submitted 11 November 2015

Accepted 26 May 2016

Published 17 June 2016

10.1126/sciadv.1501624

**Citation:** F. Yi, X. Wang, S. Niu, S. Li, Y. Yin, K. Dai, G. Zhang, L. Lin, Z. Wen, H. Guo, J. Wang, M.-H. Yeh, Y. Zi, Q. Liao, Z. You, Y. Zhang, Z. L. Wang, A highly shape-adaptive, stretchable design based on conductive liquid for energy harvesting and self-powered biomechanical monitoring. *Sci. Adv.* **2**, e1501624 (2016).

This article is published under a Creative Commons license. The specific license under which this article is published is noted on the first page.

For articles published under [CC BY](#) licenses, you may freely distribute, adapt, or reuse the article, including for commercial purposes, provided you give proper attribution.

For articles published under [CC BY-NC](#) licenses, you may distribute, adapt, or reuse the article for non-commercial purposes. Commercial use requires prior permission from the American Association for the Advancement of Science (AAAS). You may request permission by clicking [here](#).

***The following resources related to this article are available online at  
<http://advances.sciencemag.org>. (This information is current as of June 22, 2016):***

**Updated information and services**, including high-resolution figures, can be found in the online version of this article at:

<http://advances.sciencemag.org/content/2/6/e1501624.full>

This article **cites 36 articles**, 2 of which you can be accessed free:

<http://advances.sciencemag.org/content/2/6/e1501624#BIBL>

*Science Advances* (ISSN 2375-2548) publishes new articles weekly. The journal is published by the American Association for the Advancement of Science (AAAS), 1200 New York Avenue NW, Washington, DC 20005. Copyright is held by the Authors unless stated otherwise. AAAS is the exclusive licensee. The title *Science Advances* is a registered trademark of AAAS